Proceedings of the CTD 2022
PROC-CTD2022-31
January 18, 2023

Real-time alignment procedure at the LHCb experiment for Run 3

Florian Reiss

On behalf of the LHCb collaboration,
Department of Physics
University of Manchester, United Kingdom

ABSTRACT

The LHCb detector at the LHC is a general purpose detector in the forward region with a focus on studying decays of c- and b-hadrons. For Run 3 of the LHC, LHCb will take data at an instantaneous luminosity of $2 \times 10^{33}\,\mathrm{cm}^{-2}s^{-1}$. To cope with the harsher data taking conditions, LHCb will deploy a purely software based trigger with a 30 MHz input rate. The software trigger at LHCb is composed of two stages: in the first stage the selection is based on a partial event reconstruction, while in the second stage a full event reconstruction is used. This gives room to perform a real-time alignment and calibration after the first trigger stage, allowing to have the most precise detector alignment in the second stage of the trigger. The framework and the procedure for a real-time alignment of the LHCb detector in Run 3 are discussed from both the technical and operational point of view. Specific challenges of this strategy and foreseen performance are presented.

PRESENTED AT

Connecting the Dots Workshop (CTD 2022)
May 31 - June 2, 2022

1 Introduction

The LHCb Run 3 detector [1], currently being commissioned to take data during Run 3 of the Large Hadron Collider (LHC), is a general-purpose detector in the forward direction. The LHCb Run 3 detector employs a purely software-based trigger processing events at the non-empty proton-proton collision rate of 30 MHz. During Run 2, an alignment and calibration procedure in real-time has been pioneered [2]. This approach is critical for Run 3, as it is necessary for pure selections, which reduce the final output bandwidth of the trigger. In addition, having the most precise alignment available at the trigger stage ensures a fully consistent data processing chain [3].

The tracking system of the LHCb Run 3 detector providing a measurement of the momentum of charged particles consists of the Vertex Locator (VELO) [4] around the interaction region, the Upstream Tracker (UT) before, and the Scintillating Fibre tracker (SciFi) [5] after the magnet. The proton-proton interactions points (PVs) are reconstructed using tracks in the VELO. The muon system at the end of the detector reconstructs and identifies muons. Particle identification is provided by two ring-imaging Cherenkov detectors (RICH1 and RICH2) and the electronic and hadronic calorimeters (ECAL and HCAL).

2 Alignment tasks and performance

The alignment procedure consists of aligning the tracking system and the RICH mirrors. The alignment of the tracking detectors (VELO, UT, SciFi, Muon) is performed using reconstructed tracks by minimizing the χ^2 of all tracks with respect to the alignment parameters α, with

$$\begin{aligned} \chi^2 &= r^T V^{-1} r \\ r &= m - h(x, \alpha), \end{aligned} \tag{1}$$

where r are the residuals of the tracks defined as the difference between measurements m and the track model h, which depends on the track parameters x and the alignment parameters α, and V is the measurement covariance matrix. The alignment parameters describe the three translation (T_x, T_y, T_z) and three rotation (R_x, R_y, R_z) degrees of freedom of each alignable detector element.

The minimization is performed in an iterative procedure using the Newton–Raphson method by calculating the first and second derivatives of χ^2 with respect to the alignment parameters α. A new set of alignment parameters α_1 is obtained by

$$\begin{aligned} \frac{d\chi^2}{d\alpha} &= 2 \sum_{tracks} \frac{dr}{d\alpha}^T V^{-1} r, \\ \frac{d^2\chi^2}{d\alpha^2} &= 2 \sum_{tracks} \frac{dr}{d\alpha}^T V^{-1} R V^{-1} \frac{dr}{d\alpha}, \\ \alpha_1 &= \alpha_0 - \left(\frac{d^2\chi^2}{d\alpha^2} \right)^{-1} \Bigg|_{\alpha_0} \frac{d\chi^2}{d\alpha} \Bigg|_{\alpha_0}, \end{aligned} \tag{2}$$

where α_0 are the initial alignment parameters and R is the covariance matrix of the residuals. The convergence criterion is defined by $\Delta\chi^2 < 25$ for each mode and $\frac{\Delta\chi^2_{tot}}{ndof} < 4$ for the total change in χ^2 and total number of degrees of freedom $ndof$, where the change in χ^2 can be calculated from the difference in alignment parameters

$$\Delta\chi^2 = -\Delta\alpha^T Cov(\alpha)^{-1} \Delta\alpha. \tag{3}$$

This procedure uses the same track states obtained from a Kalman filter as are used in the track reconstruction, ensuring consistency between alignment and reconstruction [6]. Further, it allows to add vertex and mass constraints [7] to improve the alignment quality.

The typical samples used for the tracker alignment during Run 2 consisted of 50000 minimum bias events for the VELO alignment, where proton-proton collisions as well as proton-gas interactions were used. The

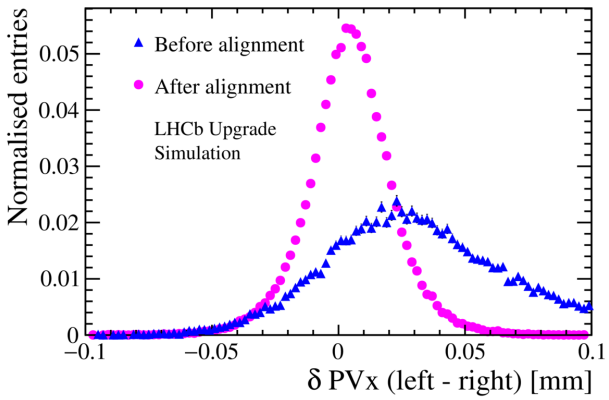

Figure 1: Difference between x positions of the reconstructed primary vertices reconstructed with tracks in each VELO half [8].

sample used for the downstream tracking system was around 70000 $\mathcal{D}^0 \to K\pi$ decays and around 200000 $J/\psi \to \mu^+\mu^-$ decays for the muon system alignment, which are expected to be collected within minutes and hours respectively in Run 3.

VELO alignment

The alignment of the VELO is of particular importance, as it is moved from a safe position while the LHC beams are injected (29 mm distance from the beamline), to a distance of 5.1 mm to the beamline when stable beams are declared.

To check the quality of the VELO alignment, the difference of the position of reconstructed PVs using only tracks in the left and right VELO halves can be used. A distribution not centered around zero would indicate a relative misalignment of the two VELO halves. The difference in x with a large initial misalignment and after the alignment procedure has converged, obtained from simulation, is shown in Fig 1.

To evaluate the precision of the VELO alignment, studies on simulated samples of a perfectly aligned detector are performed. A random initial misalignment is generated, reflecting the expected misalignment at the beginning of data-taking estimated by the detector survey accuracy, and the iterative alignment procedure is performed until it has converged. By repeating this with independent sets of initial misalignments, the final values of the alignment parameters can be studied. The bias and precision of the procedure can be estimated by the mean and width of the residual misalignment for each alignment parameter. The results of this study for the $x-$translation degree of freedom of the modules of the left VELO half are shown in Fig. 2. The initial misalignment, drawn from a Gaussian distribution with zero mean and a width of 5 µm, is compensated for by the alignment procedure, which is seen to be unbiased and to have a precision of about 1 µm, similar to what was achieved in Run 2 [9].

SciFi alignment

The alignment of the SciFi is essential to achieve the best-possible momentum resolution of charged-particle tracks. The first studies of the expected accuracy of the SciFi alignment are performed by adding a random input misalignment for the T_x degree of freedom to each SciFi module before executing the alignment procedure. The input misalignments are drawn from a Gaussian distribution with mean zero and a width of 100 µm. The input and residual misalignments after running the alignment procedure are shown in Fig. 3. The alignment can compensate for the input misalignments, reducing the standard deviation of the alignment parameters to 50 µm. This presents one of the first studies of the accuracy of the SciFi alignment. It is expected to further be improved by using a larger sample size and adding additional constraints in the alignment procedure. In particular, employing mass constraints, for example by using the abundant

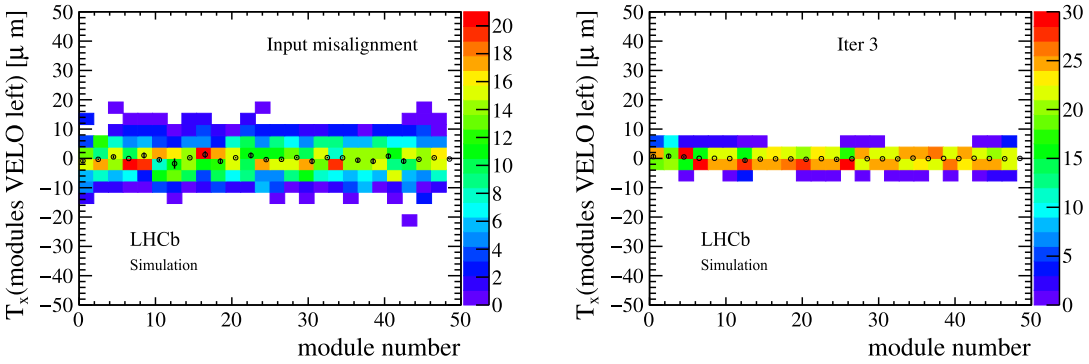

Figure 2: The input (left) and residual (right) misalignments for the T_x degree of freedom of the modules of the left VELO half [10]. Each entry corresponds to a toy with a randomly generated input misalignment and a residual misalignment after the alignment procedure has converged.

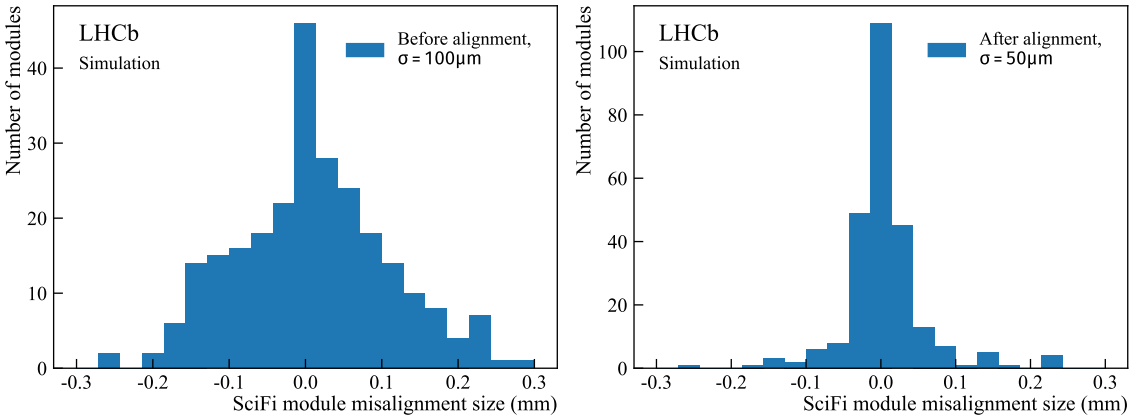

Figure 3: The input x-translation misalignment for the SciFi modules (left) and the residual misalignment (right) after running the alignment procedure [10].

$D^0 \to K\pi$ and $J/\psi \to \mu^+\mu^-$ decays, can improve the quality of the SciFi alignment.

RICH mirror alignment

The RICH mirror alignment is performed by creating histograms of the difference ($\Delta\theta_C$) of each detected photon's reconstructed Cherenkov angle and its expected Cherenkov angle, inferred from the intersection point of the charged particle with the RICH material and its measured momentum, in bins of the azimuthal angle (ϕ) about the projected track position on the photodetector plane. By fitting the $\Delta\theta_C$ distribution and correcting for deviations of its mean value from zero in each ϕ bin, the RICH mirrors can be aligned. An example of a distribution before and after the mirror are alignment is shown in Fig .4.

3 Real-time alignment and calibration

The real-time alignment and calibration is performed at the beginning of each LHC fill. The software trigger consist of two stages (HLT1 and HLT2) [11]. The first stage HLT1 employs a partial event reconstruction. Dedicated trigger lines are used to select events, which serve as input sample for the alignment procedure. Events selected by HLT1 are stored on a buffer. This allows the collection of enough events and gives enough time for the alignment and calibration procedure to run before HLT2 is executed. The HLT2

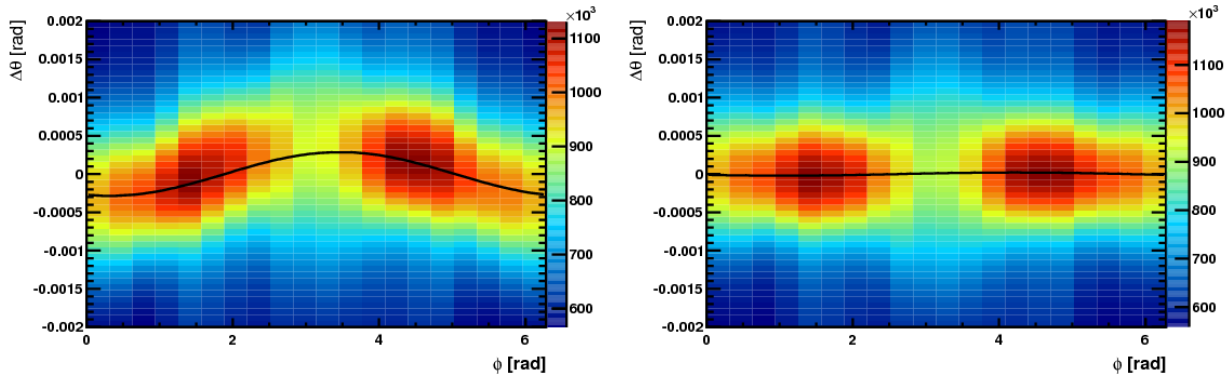

Figure 4: $\Delta\theta_C$ plotted as a function of the azimuthal angle ϕ for one side of the RICH 2 detector. The left-hand plot is prior to alignment, and shows a dependency of the angle θ_C on the angle ϕ. The right-hand plot is after the alignment correction, and $\Delta\theta_C$ is uniform in ϕ [12].

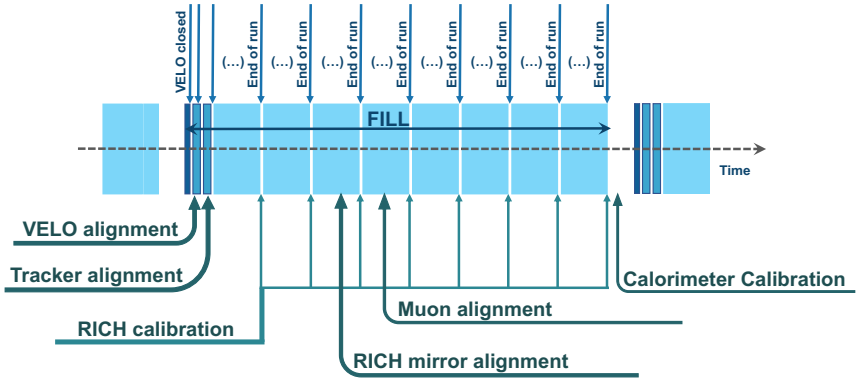

Figure 5: Real-time alignment and calibration tasks for Run 3, executed for each fill. The ordering from left to right indicates the expected amount of time each task takes, from shortest to longest.

performs a full event reconstruction including also particle identification information to make the final decision which events to keep. In this way, HLT2 can use the most recent and most precise alignment and calibration constants to achieve a reconstruction and selection performance with the best precision. This makes re-running the reconstruction offline unnecessary and results in cleaner selections with less background contributions, reducing the output bandwidth of HLT2. As the alignment of the tracking detectors can be executed within a short amount of time (order of minutes), their updated constants are also propagated to HLT1.

The foreseen real-time alignment and calibration tasks are illustrated in Fig. 5. The tracking system and the RICH mirrors are aligned using the procedure described in the previous section, the calibration is described below. After the alignment procedure has converged, it is checked if an update is necessary by comparing the previous and updated constants. If the differences are not significant, the old constants are kept to avoid changing the constants too often due to statistical fluctuations. For illustration, the variation of the $x-$ and $y-$translation constants for the VELO halves during the 2018 data-taking period is shown in Fig. 6. The VELO is expected to have frequent updates due to the movement during the closing procedure at the start of each fill.

To perform the tracking alignment on the event-filter farm, where the HLT2 processes are executed, and to achieve better timing performance, the execution of the alignment procedure is split into two parts - *Analyzer* and *Iterator*. The Analyzer reads the current alignment constants, reconstructs tracks and calculates the derivatives from Eq. 2 and saves them to a binary file. Since the event processing is independent, the

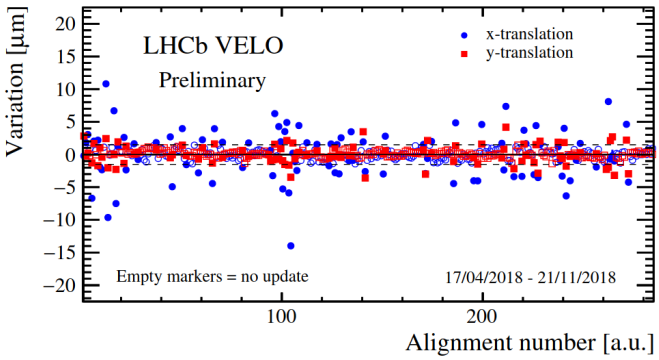

Figure 6: Stability of the translation along the x-axis (T_x) and along the y-axis (T_y) alignment constants of the VELO halves during 2018 data taking. Each point is obtained running the real-time alignment procedure and shows the difference between the initial and updated alignment constants [14].

Analzyer can be split up over multiple processes and threads. Once the Analyzer processes have finished, the Iterator collects the derivative files and performs the minimization step. New constants are written out and an update is triggered if necessary. The RICH alignment is organized in a similar way.

For Run 3, the Analyzer can utilize the multi-threaded reconstruction. This has the advantage that the alignment can be executed using fewer nodes of the event-filter farm. For each node in the event-builder farm (163 in total), there will be one node on the event-filter farm prioritizing the Analyzer tasks. This will make the distribution of the input data over the Analyzer nodes easier, as one event-builder node provides its collected sample to one Analyzer node. Due to the improvements in reconstruction throughput from multi-threading, it is expected that the alignment will run on a similar time-scale as in Run 2, even though fewer nodes are employed.

The alignment task is implemented as finite-state machine steered by the central Run Control. A scheme of the workflow is shown in Fig. 7. At the start, both Analyzer and Iterator processes are launched and the Analyzers begin with the reconstruction, while the Iterator is idling. Once the reconstruction and writing of the files with the derivatives is completed, the Iterator receives a signal to collect the files and to perform the minimization. Then it checks for convergence and triggers the continuation or completion of the alignment procedure. Once convergence is achieved, the new constants are compared with the initial ones. If the difference between them is significant, the updated constants are added to a database to be picked up by HLT2 (and HLT1 in case of the constants of the tracking system). The limits, which trigger an update, need to be carefully chosen to avoid too many updates from statistical fluctuations while still being sensitive to small misalignments. The alignment of the tracking system is expected to be completed within minutes. The RICH mirror alignment, which is not necessary for HLT1, can take more time, in the order of hours. Updates to the alignment constants of the muon stations are expected to be rare and only to be necessary after a technical intervention.

The real-time calibration consists of evaluating the refractive index that depends on the RICH temperature and gas pressure, which is evaluated on a per run basis*, and an absolute calibration of the ECAL high voltage, which was updated once per month during Run 2. For the ECAL, the calibration is performed by analyzing the $\pi^0 \to \gamma\gamma$ decay mass distribution in each calorimeter cell. From the shift of the π^0 mass peak from the known position the needed adjustment of the high voltage to compensate the aging of the detector can be estimated. This allows to optimize the calorimeter performance, as illustrated in Fig. 8 for Run 2 data, and its stability over time.

*a LHCb run corresponds to up to an hour of data-taking

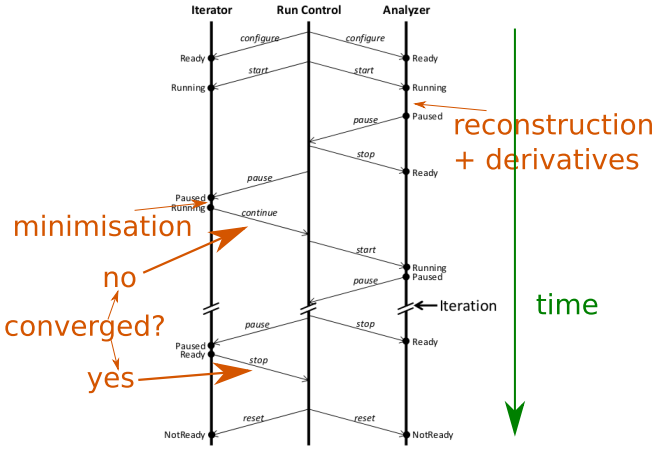

Figure 7: Illustration of the Analyzer and Iterator processes for the tracker alignment steered by the Run Control.

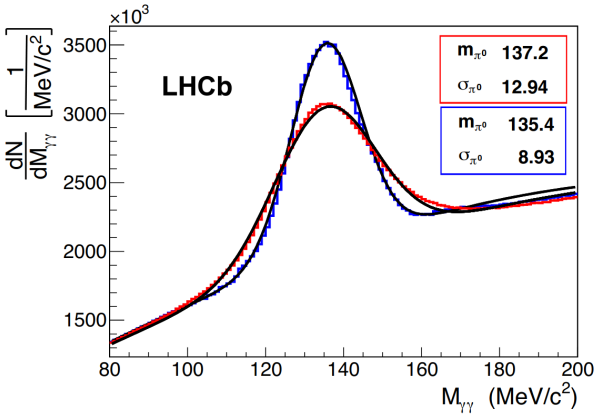

Figure 8: Invariant mass distribution for $\pi^0 \to \gamma\gamma$ candidates upon which the fine calibration algorithm is applied in Run 2. The red curve corresponds to the distribution before applying the method, while the blue curve is the final one. Values in the red (blue) box are the mean and sigma of the signal peak distribution in MeV/c^2 before (after) applying the fine calibration method [13].

4 Conclusions

During Run 2, a fully automated real-time alignment and calibration procedure was pioneered by the LHCb collaboration. This approach is essential for Run 3, where the trigger is purely software-based, to achieve the best possible physics performance of the experiment. The alignment procedure profits from the gains in reconstruction throughput achieved for HLT2, especially from multi-threading, ensuring that it can be executed in a timely manner. The system is currently being built up and will be tuned over time with feedback from taking real data.

ACKNOWLEDGEMENTS

The author would like to express gratitude to the LHCb computing, online, DPA and simulation teams for their support and for maintaining the software without which the presented work would not have been possible.

References

[1] LHCb collaboration, "Framework TDR for the LHCb Upgrade: Technical Design Report," CERN-LHCC-2012-007

[2] R. Aaij *et al.* [LHCb], "Design and performance of the LHCb trigger and full real-time reconstruction in Run 2 of the LHC," JINST **14**, no.04, P04013 (2019) doi:10.1088/1748-0221/14/04/P04013 [arXiv:1812.10790 [hep-ex]]

[3] "Computing Model of the Upgrade LHCb experiment," CERN-LHCC-2018-014.

[4] LHCb collaboration, "LHCb VELO Upgrade Technical Design Report," CERN-LHCC-2013-021.

[5] LHCb collaboration, "LHCb Tracker Upgrade Technical Design Report," CERN-LHCC-2014-001.

[6] W. Hulsbergen, "The Global covariance matrix of tracks fitted with a Kalman filter and an application in detector alignment," Nucl. Instrum. Meth. A **600**, 471-477 (2009) doi:10.1016/j.nima.2008.11.094 [arXiv:0810.2241 [physics.ins-det]].

[7] J. Amoraal, J. Blouw, S. Blusk, S. Borghi, M. Cattaneo, N. Chiapolini, G. Conti, M. Deissenroth, F. Dupertuis and R. van der Eijk, *et al.* "Application of vertex and mass constraints in track-based alignment," Nucl. Instrum. Meth. A **712**, 48-55 (2013) doi:10.1016/j.nima.2012.11.192 [arXiv:1207.4756 [physics.ins-det]].

[8] LHCb collaboration, " First study of the VELO pixel 2 half alignment," LHCB-FIGURE-2019-003.

[9] S. Borghi [LHCb], "Novel real-time alignment and calibration of the LHCb detector and its performance," Nucl. Instrum. Meth. A **845**, 560-564 (2017) doi:10.1016/j.nima.2016.06.050

[10] LHCb collaboration, "VELO and SciFi alignment accuracy studies for Run 3," LHCB-FIGURE-2022-006.

[11] "LHCb Trigger and Online Upgrade Technical Design Report," CERN-LHCC-2014-016.

[12] M. Adinolfi *et al.* [LHCb RICH Group], "Performance of the LHCb RICH detector at the LHC," Eur. Phys. J. C **73**, 2431 (2013) doi:10.1140/epjc/s10052-013-2431-9 [arXiv:1211.6759 [physics.ins-det]].

[13] C. Abellán Beteta, A. Alfonso Albero, Y. Amhis, S. Barsuk, C. Beigbeder-Beau, I. Belyaev, R. Bonnefoy, D. Breton, O. Callot and M. Calvo Gomez, *et al.* "Calibration and performance of the LHCb calorimeters in Run 1 and 2 at the LHC," [arXiv:2008.11556 [physics.ins-det]].

[14] LHCb collaboration, "2018 Alignment stability plots," LHCB-FIGURE-2019-015.